Int. J. Electrochem. Sci., 13 **(2018)** 4911 – 4922, doi: 10.20964/2018.05.82

International Journal of
ELECTROCHEMICAL
SCIENCE
www.electrochemsci.org

Study on the Galvanic Corrosion Behavior of Q235 /Ti Couple in Artificial Seawater

Xiaodong Zhang[1], *Xiaoqing Du*[2,*] *Shaowei Feng*[1], *Zhao Zhang*[2,*]

[1] MIUR, Naval University of Engineering, Wuhan 430033, People's Republic of China
[2] Department of Chemistry, Zhejiang University, Hangzhou 310027, People's Republic of China
[*]E-mail: amyzju88@163.com; eaglezzy@zju.edu.cn

Received: 26 January 2018 / *Accepted:* 27 February 2018 / *Published:* 10 April 2018

The corrosion behavior of Q235/Ti galvanic couple in the artificial seawater has been investigated by using electrochemical impedance spectroscopy (EIS), electrochemical noise (EN) and scanning electron microscope (SEM) techniques. The results show that the whole corrosion process of Q235/Ti galvanic couple should be divided into three stages by using EIS technique, whereas the same corrosion process can only be divided into two stages by using EN technique. There exists good relationship between the charge transfer resistance (R_{ct}) obtained from EIS technique and the corrosion index S_E obtained by EN technique. EN technique is more sensitive to pitting corrosion than EIS technique, and can be used to distinguish the main corrosion type.

Keywords: Q235/Ti couple; Galvanic corrosion; Electrochemical impedance spectroscopy; Electrochemical noise; Maximum entropy method

1. INTRODUCTION

In the design of many industrial projects, many materials need to combine with others to obtain the desired performance [1]. During the combination, galvanic corrosion is inevitably happened [1-3].

Galvanic corrosion is an enhanced corrosion [4], which easily occurs when two or more different metals or alloys are in electrical contact [5.6] due to the micro-macroscopic cells induced by their heterogeneities in the presence of electrolyte [3.7]. In the two contacted metals, the metal with more positive corrosion potential acts as cathode and its corrosion rate will be reduced, while the other one with more negative potential acts as anode, which corrosion will be accelerated [1]. So far, galvanic corrosion is very common in infrasturcture and industrials [8], and has been studied by many researchers [1-8]. The galvanic corrosions of Mg alloy [9,10], Al alloy [4,11], steel [12-14] in the solutions containing Cl^-, S^{2-} [12], Br^- [15,16] have attracted most attentions.

The traditional techniques used for investigating galvanic corrosion are weight-loss [4,17], potentiodynamic polarization [7,12,18], and zero resistance ammeter (ZRA) [12,18] and so on. By using these techniques, the corrosion parameters such as free corrosion potential, polarization potential, galvanic current and galvanic potential can be determined.

Nowadays, it is well accepted that electrochemical impedance spectroscopy (EIS) as a very useful electrochemical measurement could supply us with kinetic information about many electrochemical processes [19], while electrochemical noise (EN) technique has been widely used to study both the materials corrosion [20-23] and electroplating behaviors [24]. However, these methods, especially EN technique, have not yet been widely adopted in the studies of galvanic corrosion. Moreover the characteristics and the relationship of the two methods (EIS and EN) has not been studies systematically.

The aim of this work is to investigate the galvanic corrosion behavior of Q235 steel/titanium couple in the solutions artificial for the seawater of south China, especially by using EIS and EN techniques and also clarify respective characteristics of the two techniques in galvanic corrosion researches.

2. EXPERIMENTAL

The electrode for galvanic corrosion (designated as EGC) was prepared by embedding Q235 steel column in the titanium alloy (Ti) cylinder with inner and outer diameters of 0.4 and 0.56 cm, respectively. Thus, the exposed area of each metal was equal to 0.13 cm^2. Then the coupled electrode was connected respectively to a copper wire at one end, encapsulated using polytetrafluoroethylene (PTFE) with the other end exposed as the working surface. Before experiments, the working surface was polished by abrasive papers through 500-1200-grade and velvet, washed by distilled water and degreased by acetone.

Table 1. Chemical compositions of the artificial seawater

Species	Cl^-	Br^-	CO_3^{2-}	SO_4^{2-}	Na^+	K^+	Mg^{2+}	Ca^{2+}
Content (mg/l)	20237.2	72.9	1066.3	3237.2	11131.5	423	1366.6	650.4

All tests were carried out in the artificial seawater whose main components are listed in Table 1. The artificial seawater was prepared using analytic chemical reagents and double-distilled water, the latter was further purified with a Milli-Q purification system (Millipore, resistivity, 18.2 MΩ cm).

Electrochemical impedance spectra (EIS) were recorded with an impedance measurement apparatus (PARSTAT 2273, Advanced Electrochemical System) at the rest potential, the applied sinusoidal voltage amplitude was 5 mV and the sweep always initiated from the frequency of 100 kHz to 0.01 Hz. EIS tests were performed at different immersion time in a conventional three-electrode compartment cell. The coupled electrode prepared above used as the working electrode, a large platinum foil was used as auxiliary electrode and a saturated calomel electrode (SCE) was employed as

the reference. Electrochemical noise (EN) was monitored as a function of time between the working electrode and SCE using a Powerlab/4sp apparatus (made in Australia), which was controlled by Chart4 software using the Windows XP operating system. This equipment allows resolutions of 1 μV for voltage signals and 1 pA for current signals. EN data of 4096 points was collected at 4 points/s each time. These conditions define a frequency window in which most usual corrosion processes can be detected. The analytical results for maximum entropy method (MEM) technique were obtained by specific data technique.

During the above experiments, the surfaces of the samples at different immersion time were observed using scanning electron microscope (SEM, Hitachi SU70). All electrochemical tests were conducted at the temperature of about (30 ± 2) ºC, and all potentials were referred to SCE unless otherwise stated.

3. RESULTS AND DISCUSSION

The EGC corrosion behavior of Q235/Ti is first investigated using EIS technique, and some typical EIS plots are shown in Fig.1. In order to clearly see the change trend of EIS plots, Fig.1 is divided into three parts. From Fig.1, it can be seen that all centers of the capacitive circles are below the real axis, which indicates that the corrosion process of Q235/Ti EGC is controlled by charge-transfer process under our experimental conditions.

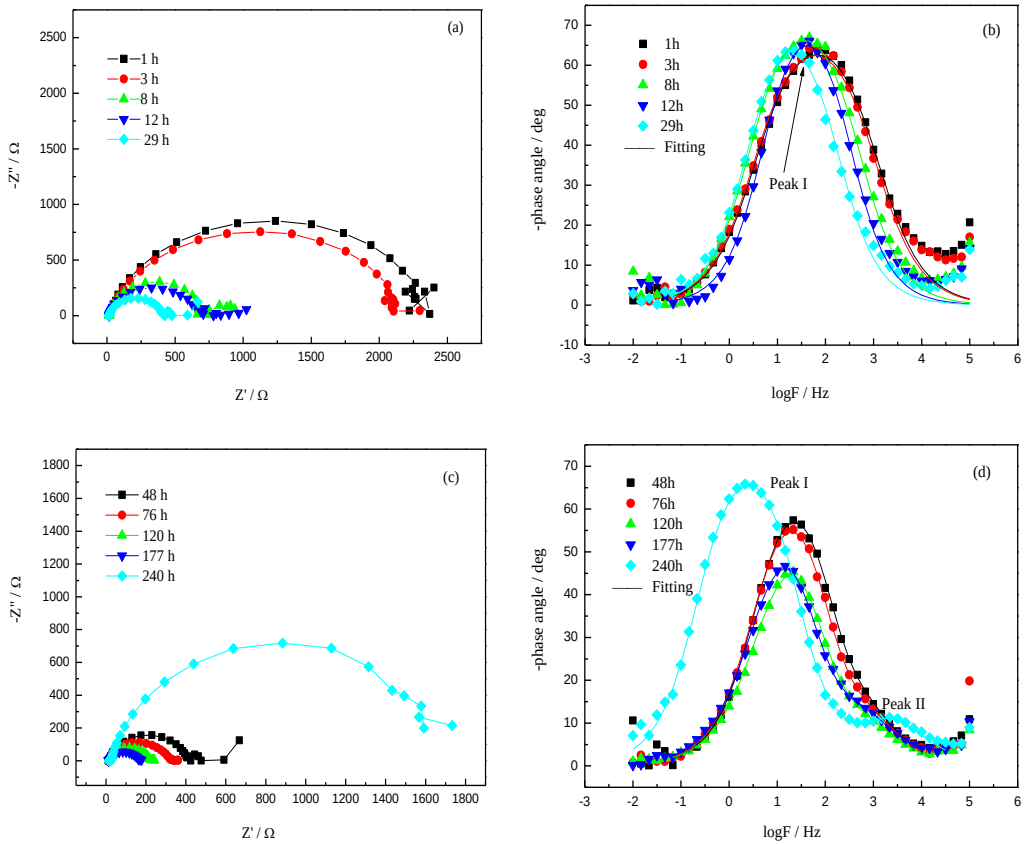

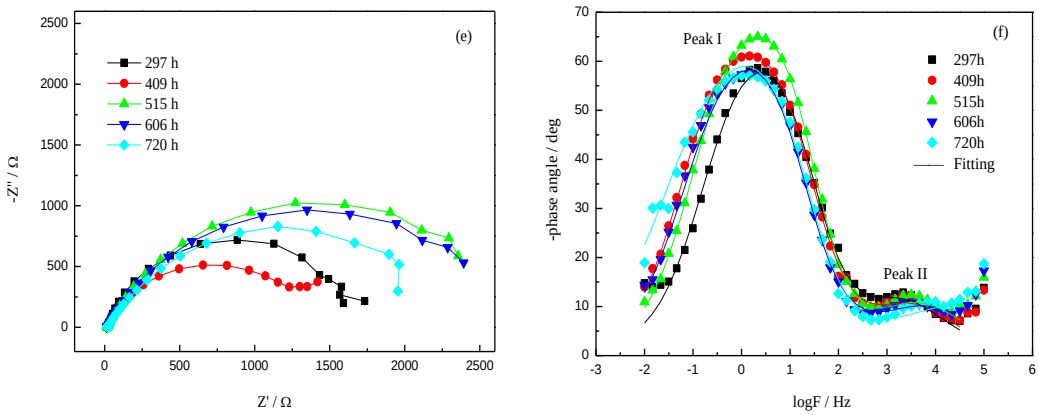

Figure 1. Nyquist(a, c, e) and Bode (b, d, f)plots of Q235/Ti EGC corroding in the artificial seawater at different immersion time.

When the corrosion time is shorter than 76 h, only one distinct phase-angle peak (Peak I) is observed in the high frequency domain except the data drift in the ultra-high frequency region. The latter phenomenon has been ascribed either to the atomic scale inhomogeneities (rather than the geometry roughness of the solid electrode) [25], or the effect of reference electrode geometry/position [26], or the high resistance capillary effect of the reference electrode [27]. Both the peak height of the phase-angle (Peak I) and the diameter of the corresponding capacitive loop decrease with immersion time (< 76 h), which indicates the more uneven distribution of corrosion current on the corroding surface [28].

In the time range from 76 h to 177 h, both the peak height of Peak I and the diameter of the corresponding capacitive loop keep in decreasing and the peak position of Peak I changes to lower frequency domain. Simultaneously, another phase-angle peak (Peak II) presenting as a shoulder of Peak I occurs in the high frequency domain. When the corrosion time is longer than 177 h, the peak height of Peak I increases but with some oscillations, which position changes to lower frequency domain, and the diameter of the corresponding capacitive loop increases also with some oscillations. Moreover, the shoulder phase-angle peak (Peak II) eventually evolves into a distinct peak (Fig. 1).

The above changes indicate that a layer of corrosion products are formed onto the Q235/Ti EGC electrode, and which structure is time dependent. For the reason that Ti acts as cathode in Q235/Ti EGC corrosion system, only the surface morphologies of the anodic Q235 are presented here. Fig. 2 clearly shows the evolution features of the morphologies of the corrosion products layer on Q235. When the corrosion time is shorter than 76 h, the corrosion products layer possesses many large cracks (Figs. 2a-2b), which is also theoretically thin and can facilitate the free transfer of the aggressive particles. In the time range from 76 h to 177 h, the corrosion products layer possesses the open leaf (loose flake) structure (Fig. 2c), which still allows the free migration of the aggressive particles. Contrarily, when the corrosion time is longer than 240 h, the corrosion products layer possesses the more and more compact globular structure (Figs. 2d-2f) and is also theoretically thicker, which can markedly hinder the free diffusion of the aggressive particles. Therefore, the accumulation of the dense corrosion products layer may be the main reason for the presentation of Peak II, and Peak I should originate from the corrosion reaction.

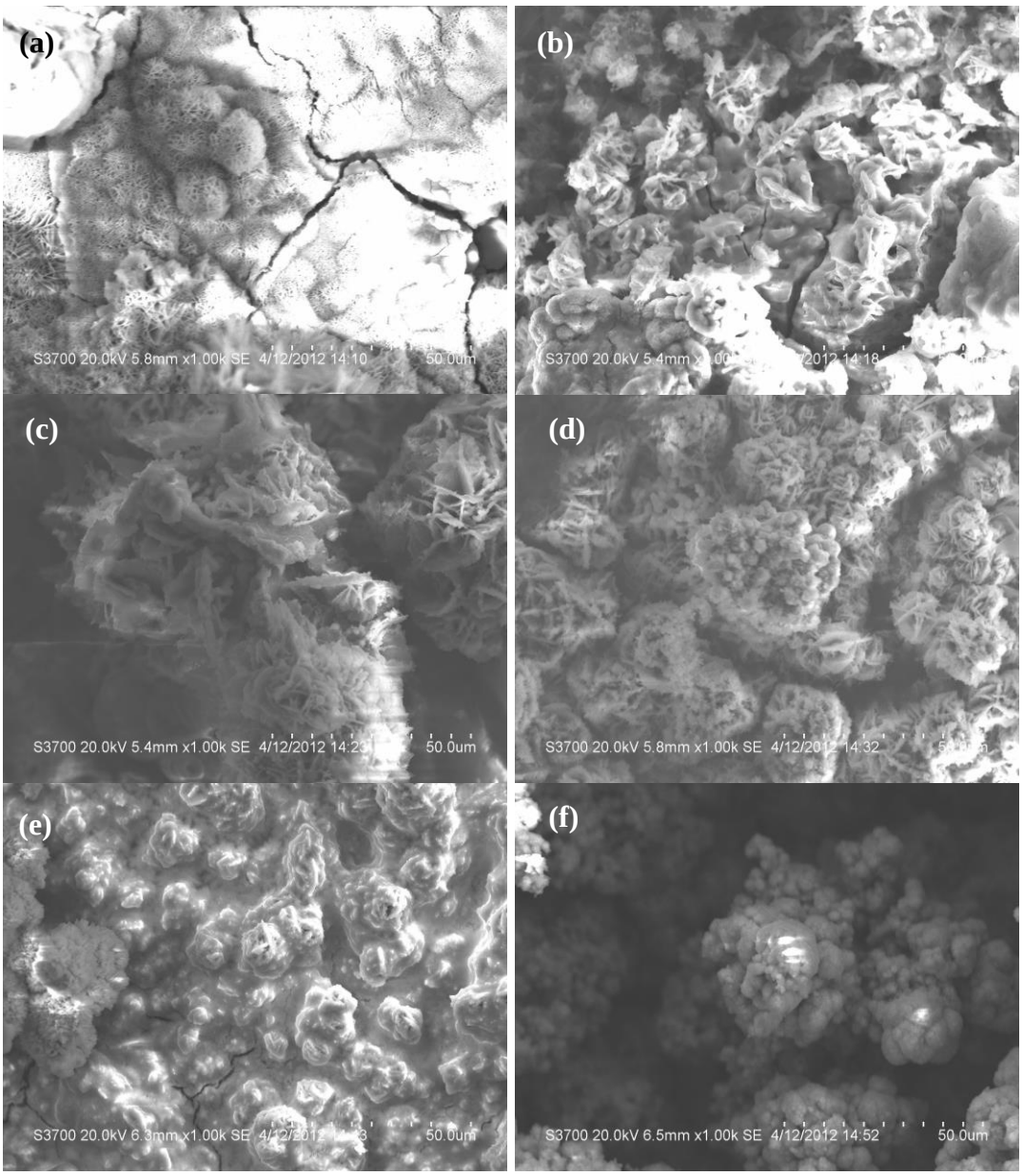

Figure 2. SEM images of Q235 in Q235/Ti EGC after corroding for different times. (a) 1h, (b) 24h, (c)120 h, (d) 240 h, (e) 480h, (f) 720h.

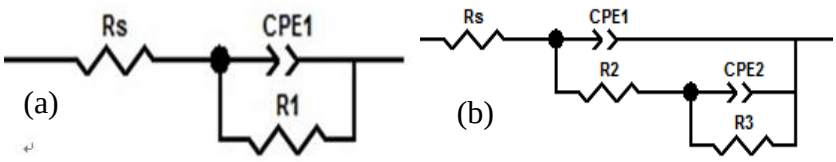

Figure 3. EECs used for simulating the impedance spectra of Q235/Ti EGC corroding in seawater.

(a) R_s is the solution resistance, *CPE*1-P is the electric double layer capacitance, *R*1 is charge transfer resistance. (b) R_s is the solution resistance, *CPE*1-P is the capacitance of outer passivating film and corrosion product layer, R_2 is the membrane resistance of outer passivaitng film and corrosion products, *CPE*2-P is the electric double layer capacitance, *R*3 is the charge transfer resistance.

According to the above analysis (especially the features of the EIS diagrams, such as the number of the phase angle peak in Bode plots) and the method developed by Wit [29, 30], the number of EIS time constant can be determined clearly. Therefore, the EIS data in Fig. 1 are analyzed using two different equivalent electrical circuit (EEC) models (Fig. 3) and the non-linear-least-square fit analysis (NLLS) software.

Table 2. The fitted results of Q235 steel/Ti EGC corroding in seawater at the first 24h (The initial stage)

Time/h	R_s/Ω	*CPE1*-*P*/μF	n_1	R_{ct}/Ω
1.0	17.25	33.4	0.82668	2291
1.5	18.07	37.5	0.81546	2180
3.0	18.13	44.4	0.80721	1964
8.0	16.82	57.5	0.86007	1589
12	15.87	76.5	0.86865	964.5
29	15.86	73.3	0.90632	688.9
48	15.31	140	0.87660	675.4

Table 3. The fitted results of Q235 steel/Ti EGC corroding in seawater from 48h to 720h (The transitory and the last stages)

Time/h	R_S/Ω	*CPE*1-*P*/μF	n_1	R_f/Ω	*CPE*2-*P*/μF	n_2	R_{ct}/Ω
76	13.22	176	0.79214	13.70	65.9	0.94993	321.4
96	12.68	214	0.76776	12.87	76.3	0.94993	291.6
120	13.89	354	0.72987	13.22	93.9	0.94993	164.8
148	12.14	296	0.74967	13.66	141	0.94993	194.5
177	11.59	399	0.71502	13.44	155	0.94993	164.8
199	11.48	528	0.67747	14.09	161	0.94993	181.0
218	11.41	623	0.67133	14.54	171	0.94993	155.1
240	15.35	686	0.74993	11.85	266	0.89477	1696
297	13.40	780	0.62034	15.03	422	0.83715	1518
337	13.92	309	0.71394	19.27	870	0.69818	1886
409	12.47	234	0.62706	12.24	564	0.82292	2903
458	12.50	210	0.63197	11.88	370	0.88814	3149
494	12.25	229	0.62457	11.26	348	0.90162	3476
515	11.67	235	0.60326	12.71	370	0.88939	2793
540	11.61	298	0.58487	13.45	362	0.88902	3266
563	10.43	315	0.53890	15.12	427	0.85075	3994
582	17.17	213	0.57504	19.50	486	0.82255	2798
606	16.83	232	0.54982	19.48	520	0.81673	2890
630	16.50	299	0.52971	17.76	538	0.81191	3265
655	15.52	263	0.51620	17.07	599	0.80052	3575
680	16.19	390	0.48173	17.95	520	0.82194	6830
703	14.82	342	0.48256	17.16	566	0.81244	6891
720	10.56	258	0.43196	22.29	627	0.80481	8266

When the immersion time is shorter than 76 h, only one time constant can be clearly determined, and therefore the EEC in Fig. 3a is used to fit the EIS plots. When the immersion time is longer than 76 h, two time constants can be determined and therefore the EEC in Fig. 3b is used to fit these EIS plots. The fitted results are shown in Table 2 and Table 3.

In order to see clearly both the evolution features of *CPE1-P* and (the charge transfer resistance) for Q235/Ti EGC corroding in the artificial seawater, the data of *CPE1-P* and *Rct* in Table 2 and Table 3 are plotted versus corrosion time and shown in Figs. 4-5. It can be seen that *Rct* decreases continuously from the initial corrosion time to 240 h, which can be mainly attributed to the autocatalytic effect of pitting corrosion in the enclosed environment [23] (Fig. 2). Meanwhile, *CPE1-P* increases due to both the increase of the real corroding surface and the relative dielectric constant of the surface layer (corrosion products are hydroxyl compounds and possess higher relative dielectric constant when compared with Q235). In the time range from 76 h to 240 h, the decreasing rate of *Rct* is smaller than that when the corrosion time is shorter than 76 h, which should be originated from the time-dependent structure of the corrosion products layer (Fig. 2), as elucidated above.

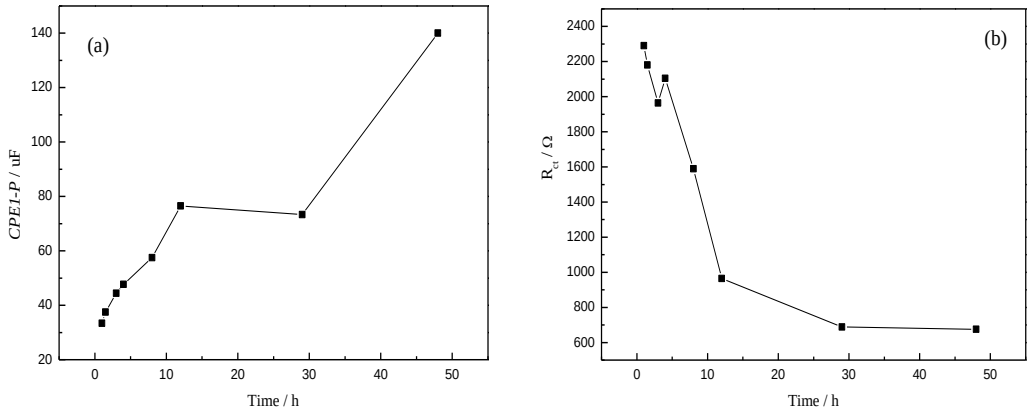

Figure 4. The evolution features of *CPE1-P* (a) and the charge transfer resistance *Rct* (b) for Q235/Ti EGC corroding in the artificial seawater (< 76 h).

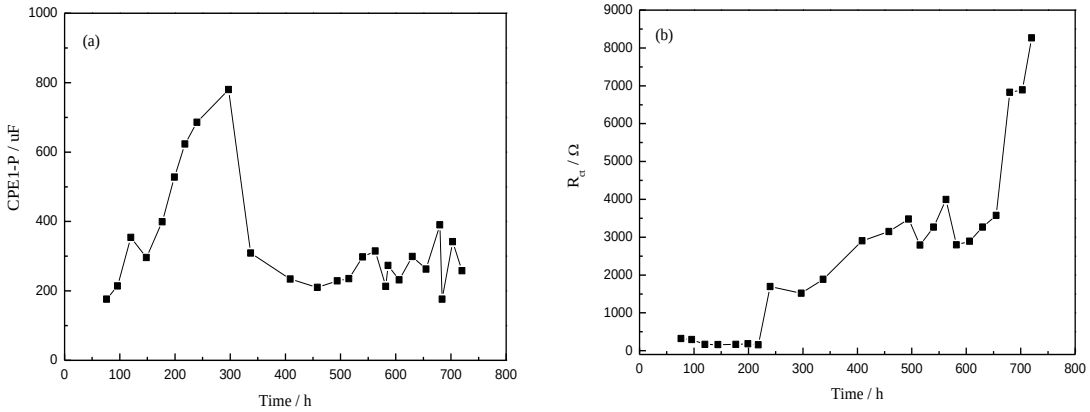

Figure 5. The evolution features of *CPE1-P* (a) and the charge transfer resistance *Rct* (b) for Q235/Ti EGC corroding in the artificial seawater (≥ 76 h).

When the corrosion time is longer than 240 h, *Rct* increases while *CPE1-P* changes oppositely due to the formation of the thicker and denser corrosion products layer, and also because that the coupled Ti is a kind of metals with high corrosion resistance.

According to the above analyses, the corrosion process of Q235 /Ti EGC can be divided into three stages, i.e, the initial stage (< 76 h), the transitory stage and the last stage (> 240 h).

Fig. 6 shows the time-domain potential noise curve (without elimination of the dc drift) of Q235/Ti EGC corroding in seawater for 722 h. The initial corrosion potential (-0.53 V) of Q235/Ti EGC is more negative than that of single Q235 steel (-0.48 V), which means that when coupled Q235 steel with Ti, the corrosion of Q235 becomes to be much easier. The corrosion potential shows the evolution trend of the initial negative drift and a subsequent increase (Fig. 6). At the end of the corrosion study, the corrosion potential of Q235/Ti EGC arrives at a relatively stable value of about -0.68V, which is same as that of single Q235 steel corroding in same seawater (not shown here).

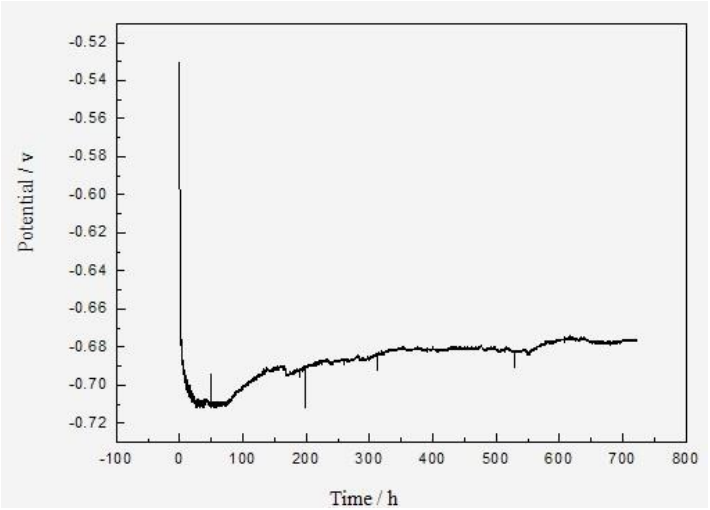

Figure 6. Time-domain potential noise of Q235/Ti EGC corroding in seawater for 722 h.

The potential noise shown in Fig.6 has been analyzed by using MEM technique [31], the obtained spectral power density plots (PSD) [32-34] are shown in Fig. 7. Based on the three characteristic parameters of the PSD curves (white noise level P_w, the cut-off frequency f_c and the high frequency linear slope k), two corrosion indexes S_E and S_G [20, 21] can be calculated as follows:

$$S_E = f_c^{\,2}\sqrt{k} \qquad (1)$$

$$S_G = \frac{W}{f_c k} \qquad (2)$$

Fig. 8 shows the evolution features of S_E and S_G with time. Fig. 8 clearly shows that the whole corrosion process of Q235/Ti EGC can be divided into two stages. In the first stage (< 240 h), S_E oscillates with large amplitude, while S_G keeps continuously decreasing. In the second stage (> 240 h), S_E keeps at a relatively small value, while S_G increases. According to our previously studies [20, 21], S_E mainly reflects the strength of the fast reaction processes (such as pitting corrosion), while S_G

reflects mainly those of slow processes (such as diffusion). The larger the S_E, the more the fast reactions (with smaller time-constant) taking place simultaneously.

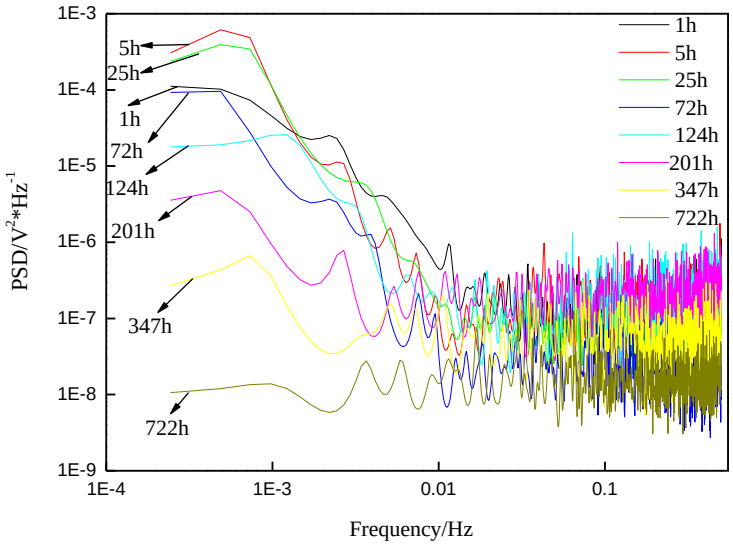

Figure 7. PSD plots of Q235/Ti EGC corroding in seawater at different time (722 h)

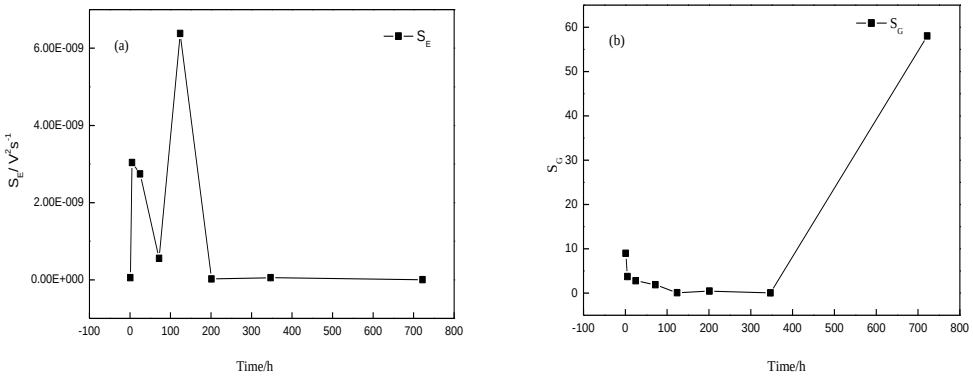

Figure 8. The S_E (a) and S_G (b) value of Q235 steel/ti corrosion in seawater at different times

Compare the variation trends of R_{ct} and *CPE1-P* (Figs. 4-5) with those of S_E and S_G (Fig. 8), it is very interesting to find that, the time domain for the large-amplitude oscillating of S_E is the same as that for the continuously decreasing of R_{ct} (< 240 h), while S_E keeps at a relatively small value when R_{ct} increases markedly (> 240 h). On the other hand, the time domain for the decreasing of S_G is also the same as that for the continuously increasing of *CPE1-P* (< 240 h), the decreasing of *CPE1-P* (> 240 h) is accompanied by the increasing of S_G.

It is well accepted that the main corrosion type of steel (including Q235) in seawater is pitting corrosion, and the charge transfer resistance (R_{ct}) is widely used to characterize the corrosion rate [35,36], therefore, the smaller the R_{ct}, the fast the pits formation. However, how to elucidate the relationship between S_G and *CPE1-P* ?

CPE1-P is directly dependent on the characteristics of the surface layer on the corroding electrode. Generally, the surface of solid (electrode) is inhomogeneous in nature and exist some active points with higher surface energy [25]. In the same corroding conditions, the active points initiate pitting corrosion preferentially. With the increasing of pitting rate, the corroding surface becomes more and more irregular (which can be proved by the decrease of $n1$ in Table 2) and consequently increases the real surface area, while the formed corrosion products covers onto the electrode (Fig. c) and theoretically thickens. The above two factors cause the increasing of *CPE1-P* (Figs. 4-5) when the corrosion time is less than 240 h. Also because of the preferential initiation of pitting corrosion of the active points on the inhomogeneous solid (electrode) surface, the aggressive particles (such as O_2 and Cl^-) must diffuse certain distance to reach these points, which results in the initial higher value of S_G (the first point in Fig. 8). With the prolongation of corrosion time (< 240 h), all the non-protective characters of the theoretically thinner corrosion products layer (with many large cracks (Figs. 2a-2b) or open leaf (loose flake) structure (Fig. 2c)), the autocatalytic effect of pitting corrosion [23] and the concentration effect of Cl^- in the pit's tip [37], make the diffusion processes of the aggressive particles much easier and result in the slowly decreasing of S_G.

When the corrosion time is long enough (>240 h), the structure of the time-dependent corrosion products layer changing from the open leaf (loose flake) structure (Fig. 2c) to the dense globular structure (Figs. 2d-2f) and some dense corrosion products blocking into the pitting holes tightly, both of them make the diffusion processes of the aggressive particles (such as O_2 and Cl^-) become more and more difficult, therefore S_G increases (Fig. 8). The synergism of the above factors also results in the annihilation of some already formed pits and the initiation of some new pits, therefore, general corrosion is the main corrosion type at this time. The general corrosion causes the solid (electrode) surface to be somewhat smooth again, thus *CPE1-P* decreases.

At the last of this paper, it should be mentioned that there exists a discrepancy when using EIS and EN techniques to study the same corrosion process of Q235/Ti EGC in the artificial seawater, respectively. According to the studies of EIS, the whole corrosion process of Q235/Ti EGC should be divided into three stages, whereas the same corrosion process can only be divided into two stages by using EN technique. This discrepancy may infer that EN technique is more sensitive to pitting corrosion, and can be used to distinguish the main corrosion type as elucidated above.

4. CONCLUSIONS

The corrosion process of Q235/Ti EGC in the static artificial seawater is charge-transfer controlled, and Q235 acts as the anode. The charge transfer resistance (R_{ct}) shows the variation trend of initial decrease (< 240 h immersion time) and subsequent increase (> 240 h immersion time), while the surface capacity (*CPE1-P*) changes oppositely. When the corrosion time is less than 240 h, the corrosion parameter S_E obtained by EN technique possesses large oscillations, and the time domain for the large-amplitude oscillating of S_E is the same as that for the continuously decreasing of R_{ct}. When the corrosion time is longer than 240 h, S_E keeps at a relatively small value while R_{ct} increases markedly. On the other hand, the time domain for the decreasing of S_G is also the same as that for the continuously increasing of *CPE1-P* (< 240 h), the decreasing of *CPE1-P* (> 240 h) is accompanied by

the increasing of S_G. The discrepancy between the results obtained by EIS and EN techniques indicates that the latter is more sensitive to pitting corrosion, and can be used to distinguish the main corrosion type.

ACKNOWLEDGEMENTS
The authors wish to acknowledge the financial supports of the National Natural Science Foundation of China (Projects: 51771173, 21073162, 21403194 and 21363018)

References

1. D. Filotás, B. M. Fernández-Pérez, J. Izquierdo, L. Nagy, G. Nagy, R. M. Souto, *Corros. Sci.*, 114 (2017) 37.
2. J. Liu, Y. Song, J. Chen, P. Chen, D. Shan, E. H. Han, *Electrochim. Acta*, 189 (2016) 190.
3. M. K. DeSantis, S. Triantafyllidou, M. Schock, D. A. Lytle, *Environ. Sci. Technol.*, 2018. DOI: 10.1021/acs. est. 7b06010.
4. Z. F. Yin, M. L. Yan, Z. Q. Bai, W. Z. Zhao, W. J. Zhou, *Electrochim. Acta*, 53 (2008) 6285.
5. H. B. Ding, L. H. Hihara, *J. Electrochem. Soc.*, 158 (2011) 118.
6. R. M. Souto, Y. Gonza′lez-Garcı, A. C. Bastos, A. M. Simoes, *Corros. Sci.*, 49 (2007) 4568.
7. A. N. AlHazaa, E. S. M. Sherif, *Int. J. Electrochem. Sci.*, 10 (2015) 4193.
8. D. L. Zhang, W. Wang, Y. Li, *Corros. Sci.*, 52 (2010) 1277.
9. P. Zhang, X. Nie, D. O. Northwood, *Surf. Coat. Technol.*, 203 (2009) 3271.
10. C. Liu, D. L. Chen , S. Bhole, X. Cao, M. Jahazi, *Mater. Charact.*, 60 (2009) 370.
11. L. Yin, Y. Jin, C. Leygraf, J. Pan, *Electrochim. Acta*, 192 (2016) 310.
12. C. F. Dong, K. Xiao, X. G. Li, Y. F. Cheng, *J. Mater. Eng. Perform.*, 20 (2011) 1631.
13. C. F. Dong, K. Xiao, X. G. Li, Y. F. Cheng, *Wear*, 270 (2010) 39.
14. A. A. Khadom, A. F. Hassan, B. M. Abod, *Process Saf. Environ. Prot.*, 98 (2015) 93.
15. V. Guinon-Pina, A. Igual-Munoz, J. García-Antón, *Corros. Sci.*, 53 (2011) 575.
16. E. Blasco-Tamarit, A. Igual-Munoz, J. García Antón, D.M. García-García, *Corros. Sci.*, 59 (2009) 1095.
17. T. Bellezze, G. Giuliani, A. Viceré, G. Roventi, *Corros. Sci.*, 130 (2018) 12.
18. J. Z. Ai, X. P. Guo, Z. Y. Chen, *Appl. Surf. Sci.*, 253 (2006) 683.
19. W. H. Leng, Z. Zhang, J. Q. Zhang, C. N. Cao, *J. Phys. Chem. B*, 109 (2005) 15008.
20. Y. Y. Shi, Z. Zhang, F. H. Cao, J. Q. Zhang, *Electrochim. Acta*, 53 (2008) 2688.
21. Y. Y. Shi, Z. Zhang, J. X. Su, F. H. Cao, J. Q. Zhang, *Electrochim. Acta*, 51 (2006) 4977.
22. F. H. Cao, Z. Zhang, J. X. Su, Y. Y. Shi, J. Q. Zhang, *Electrochim. Acta*, 51 (2006) 1359.
23. C. Cai, Z. Zhang, F. H. Cao, Z. N. Gao, J. Q. Zhang, C. N. Cao, *J. Electroanal. Chem.*, 578 (2005) 143.
24. Z. Zhang, W. H. Leng, Q. Y. Cai, F. H. Cao, J. Q. Zhang, *J. Electroanal. Chem.*, 578 (2005) 357.
25. Z. Kerner, T. Pajkossy, *Electrochim. Acta*, 46 (2000) 207
26. G. Hsieh, T.O. Mason E. J. Garboczib, L. R. Pederson, *Solid State Ionics*, 96 (1997) 153
27. J. H. Park, J. J. Park, O. O. Park, C. S. Jin, J. H. Yang, *J. Power Sources*, 310 (2016) 137.
28. A. Nishikata, Y. Ichihara, Y. Hayashi, T. Tsuru, *J. Electrochem. Soc.*, 144 (1997) 1244.
29. D. H. Van Der Weijde, E. P. M. Van Westing, J. H. W. de Wit, *Corros. Sci.*, 36 (1994) 643.
30. P. Campestrini, E. P. M. Van Westing, J. H. W. de Wit, *Electrochim. Acta*, 46 (2001) 2553.
31. Y. Hou, C. Aldrich, K. Lepkova, L. L. Machuca, B. Kinsella, Corros. Sci., 112(2016) 63.
32. J. Flis, J. L. Dawson, J. Gill, G. C. Wood, *Corros. Sci.*, 32 (1991) 877.
33. R. A. Cottis, A. M. Homborg, J. M. C. Mol, *Electrochim. Acta*, 202(2016) 277.
34. F. Mansfeld, H. Xiao, *J. Electrochem. Soc.*, 140 (1993) 2205.

35. D. J. Fang, X. H. Mao, Y. M. Zhang, *Anti-Corros. Methods Mater.*, 56(2009) 226.
36. Y. L. Cheng, Z. Zhang, F. H. Cao, J. F. Li, J. Q. Zhang, *Corros. Sci.*, 46 (2004) 1649.
37. C. S. Wu, Z. Zhang, Y. L. Cheng, J. F. Li, J. Q. Zhang, J. M. Wang, C. N. Cao, *Acta Metall. Sin.*, 17 (2004) 92.